Evaporation of Binary Sessile Drops: Infrared and Acoustic Methods To Track Alcohol Concentration at the Interface and on the Surface

Pin Chen, Malika Toubal, Julien Carlier, Souad Harmand, Bertrand Nongaillard, Maxence Bigerelle

Evaporation of Binary Sessile Drops: Infrared and Acoustic Methods To Track Alcohol Concentration at the Interface and on the Surface

Pin Chen,[†] Malika Toubal,[‡] Julien Carlier,[‡] Souad Harmand,[*,†] Bertrand Nongaillard,[‡] and Maxence Bigerelle[†]

[†]LAMIH Laboratory and [‡]IEMN DOAE Laboratory, University of Valenciennes, Valenciennes 59313, France

ABSTRACT: Evaporation of droplets of three pure liquids (water, 1-butanol, and ethanol) and four binary solutions (5 wt % 1-butanol–water-based solution and 5, 25, and 50 wt % ethanol–water-based solutions) deposited on hydrophobic silicon was investigated. A drop shape analyzer was used to measure the contact angle, diameter, and volume of the droplets. An infrared camera was used for infrared thermal mapping of the droplet's surface. An acoustic high-frequency echography technique was, for the first time, applied to track the alcohol concentration in a binary-solution droplet. Evaporation of pure alcohol droplets was executed at different values of relative humidity (RH), among which the behavior of pure ethanol evaporation was notably influenced by the ambient humidity as a result of high hygrometry. Evaporation of droplets of water and binary solutions was performed at a temperature of 22 °C and a mean humidity of approximately 50%. The exhaustion times of alcohol in the droplets estimated by the acoustic method and the visual method were similar for the water–1-butanol mixture; however, the time estimated by the acoustic method was longer when compared with that estimated by the visual method for the water–ethanol mixture due to the residual ethanol at the bottom of the droplet.

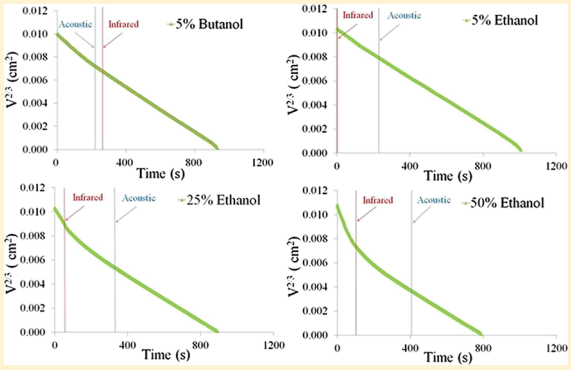

INTRODUCTION

In recent decades, many experimental[1−7] and theoretical studies[5,8−12] have investigated the process of evaporation of drops, which has a wide range of applications, for example, ink-jet printing,[13,14] DNA mapping,[15,16] combustion engineering,[17,18] and cooling systems.[19,20] Measuring the droplet parameters (contact angle, base radius, and height), using optical and infrared techniques, can contribute to full understanding of the evaporation process. Moreover, the dynamic evaporation of a binary mixture drop that can contain both a constant contact angle regime and constant contact radius regime is more complicated.

At ambient conditions, the evaporation process of water–ethanol mixture drops can be divided into three stages: the first stage conforms to the behavior of the pure volatile component; at the last stage, the drop evaporates in accordance with the less volatile component; and there is an intermediate (transitional) stage, where the contact angle clearly increases with a nearly constant volume.[21] Christy et al. also showed that the evaporation of the water–ethanol mixture sessile drop went through three distinct stages when they studied the interior flow in the droplet using particle image velocimetry (PIV) technology: (1) chaotic regime, dominated by multiple vortices driven by concentration differences as a result of the preferential evaporation of ethanol; (2) transition regime, characterized by an exponential decay of vortices with the migration of the remaining vortices toward the drop periphery and a spike of the radial velocity along the drop base; and (3) the third stage, characterized by the evaporation driving outward flow to the contact line, acting exactly the same as pure water drops.[22] During the evaporation process of the water–ethanol mixture, O'Hare and Spedding found that the evaporation rate of the water component was nearly constant, despite the continuous decrease in the actual ethanol concentration.[23] Furthermore, Liu et al. discovered that the evaporation behavior of the water–ethanol mixture drop can be more complex: ethanol did not finish thoroughly at the end of the transitional stage; rather, until the end of evaporation, part of the residual ethanol still remained in the drop. The water vapor condensed as the mixture drop began to evaporate at a high ratio of ethanol in the drop and a high vapor pressure of water in the background gas.[24]

Despite the numerous research studies performed on the evaporation of water-based binary alcohol solutions, there is still lack of understanding of the evolution of alcohol concentration during evaporation. In this study, dynamic evaporation of sessile drops of three pure liquids (water, 1-butanol, and ethanol) as well as water–1-butanol and water–ethanol mixtures was investigated using a complementary original dual-track approach combining optical and infrared techniques on the one hand and acoustics on the other hand.

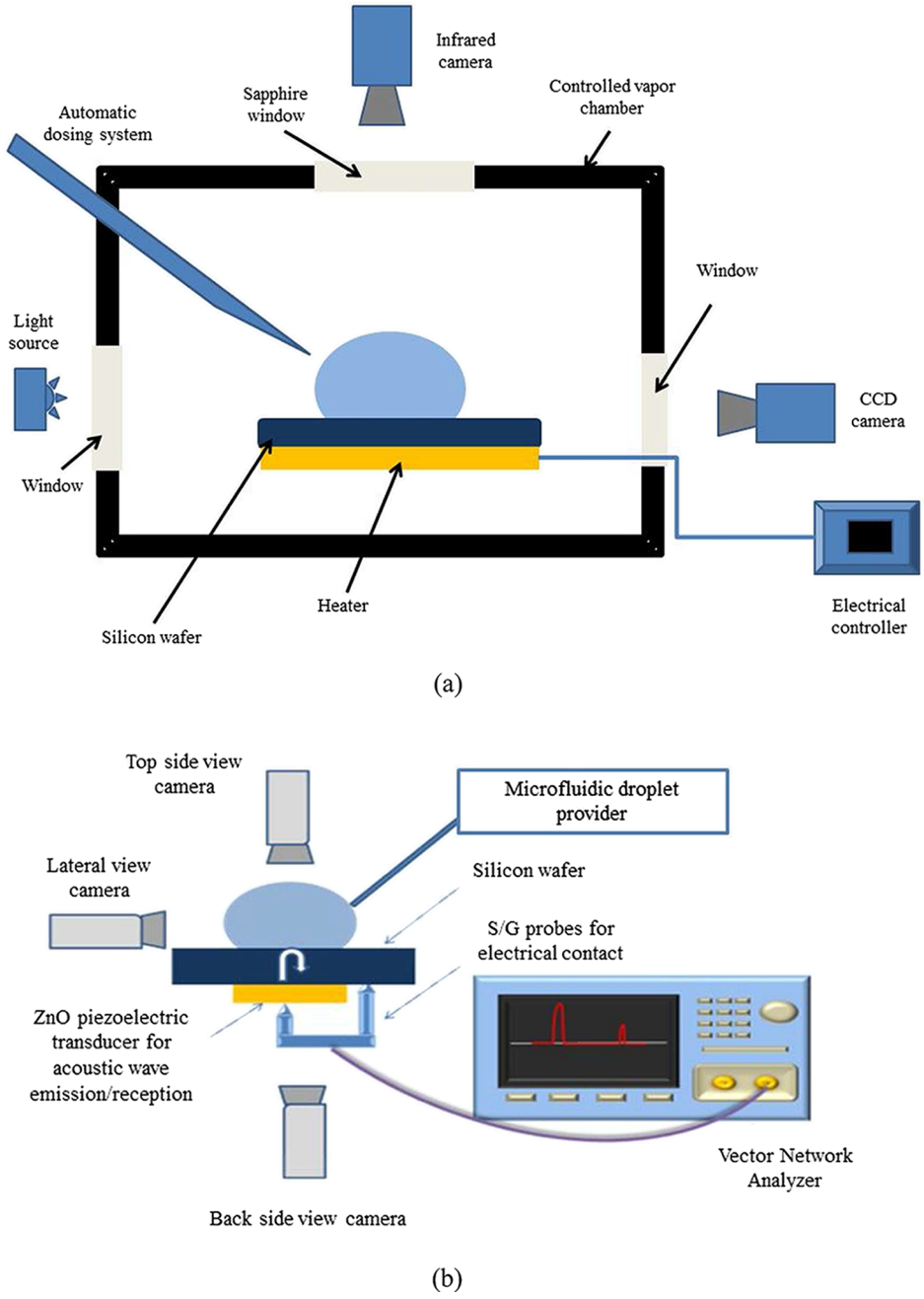

Figure 1. Schema of the experimental setup: (a) workbench of the modified Kruss Drop Shape Analyzer and infrared camera; (b) acoustic workbench.

Whereas the optical and infrared techniques provide macroscopic information of the phenomenon on the drop surface, the use of acoustics gives access to local interface exchange mechanisms at the bottom of the drop.

An acoustical method has been developed in our laboratory to characterize solid−liquid interfaces at micro-/nanometer scales. First, the focus was on the wetting of droplets of various surface tensions on hydrophobized textured structures.[25] The surface tension threshold of the droplet was correlated with the observation of the transition from the Cassie−Baxter to Wenzel state. Another targeted application was the determination of cleaning efficiency in the nanoelectronics fabrication process. The ultrasonic technique is not only used in the tracking of Cassie−Wenzel transition on microstructures during the evaporation process of a droplet on a microstructure surface[26,27] but also in nanostructures wetting characterization on periodic surfaces.[28]

In the case of binary drop evaporation, alcohol concentration tracking, which is the main interest of ultrasound techniques, is due to the high contrast of mechanical impedances between certain alcohols, such as 1-butanol and ethanol, trapped at the interfaces and liquids. Moreover, ultrasound techniques do not require any optical transparency. This sensitivity enables the monitoring of the evaporation kinetics of droplets of some water−alcohol mixtures at a plane of solid−liquid interface by the tracking of the concentration evolution at the interface between the droplet and the support. Depending on the binary alcohol concentration of the drop, the mechanical impedance of

the liquid and the acoustic reflection coefficient will be modified. Because of a pre-established calibration curve of the reflection coefficient, which depends on the alcohol concentration of the droplet, it is possible to determine the concentration of alcohol on line at the interface by the acoustic reflection coefficient measurement.

EXPERIMENTAL SETUP

Two separate devices are used, one for optical and infrared measurements and the other for acoustic reflection coefficient measurements. In both cases, the droplets are left to evaporate on the hydrophobized (100) silicon substrate treated with PFTS (perfluorodecyltrichlorosilane). Measurements are taken at a temperature of 22 °C and a mean humidity of approximately 50%. Moreover, the influence of humidity, namely 20%, 50%, and 56%, on infrared and optical measurements is considered in the case of the evaporation of pure alcohol.

Optical and Infrared Measurements. The substrates are placed in a vapor chamber (14 × 12.4 × 7.5 cm^3), in which the ambient temperature and relative humidity (RH) can be controlled (Figure 1a). The air inside of the chamber is at rest. The top of the vapor chamber has a sapphire window for the infrared camera and a hole for passing the syringe. The infrared camera (FLIR X6580SC, 640 × 512 pixels, 15 μm detector pitch) is installed on the top for infrared thermal mapping and visualization of thermal instabilities on the surface of the droplets. The exploitation of dynamic infrared videos provides a good visualization of the motion of alcohol cells on the droplet surface and consequently the alcohol life time during evaporation because water and alcohol have different emissivities. A Kruss Drop Shape Analyzer is used to measure the contact angle, volume, diameter, and height of sessile droplets during evaporation. A side-view CCD camera (Allied Vision Technologies, 780 × 580 pixels) is used to record the evaporation process of the droplets for profile analysis.

Acoustic Measurements. The measurements are made under a controlled atmosphere thanks to an air-conditioning system. A Cascade PM8 prober system is used to control the position of the S/G (signal/ground) probe at the microscale level on a piezoelectric transducer as small as 50 μm in diameter to achieve electrical measurements (Figure 1b). The specificity of the probe is the possibility to achieve an electrical contact at the backside of the wafer on which the piezoelectric transducer was fabricated. These probes are connected to a Rhode & Schwarz ZVA8 Vector Network Analyzer. The droplet is deposited on the top side of the substrate via a microfluidic device. A rear view camera is used to check the alignment of the probe and the transducer. The top view camera helps to check the correct position of the drop above the transducer surface, whereas the lateral view camera gives information of the contact angle.

The acoustic method is based on the high-frequency echography principle. A high-frequency (1 GHz) longitudinal wave is generated by ZnO piezoelectric transducers fabricated on the backside of the (100) silicon substrate on which the solid−liquid interface is characterized. The diameter of the ZnO transducers is about 250 μm. The thickness of the silicon substrate is about 500 μm. The $S_{11}(f)$ scattering parameter (ratio of the complex amplitudes of the reflected and incident signals) is measured by using a Suss Microtec probe coupled with a Hewlett Packard 8753 Vector Network Analyzer. This parameter is the result of two separate contributions, electric S_{11}^{el} and acoustic S_{11}^{ac}

$$S_{11}(f) = S_{11}^{el} + KS_{11}^{ac} \tag{1}$$

where K refers to the electromechanical conversion effects at the interfaces. The S_{11}^{ac} parameter results from the superposition of the acoustic waves generated from all the reflected waves at the interface.

An inverse Fourier transform applied on the $S_{11}(f)$ signal makes it possible to separate the acoustic contribution from the electric one. These two signal contributions are separated by a delay corresponding to the propagation in the substrate. The signal in the time domain, windowed on the useful echo corresponding to the first reflected echo, is then processed to determine the reflection coefficient.

From a theoretical point of view, a plane of the acoustic wave propagating at normal incidence at an interface separates two media of acoustic impedances Z_1 and Z_2; the absolute value of the reflection coefficient R in amplitude can be calculated using the following equation

$$|R| = \frac{Z_2 - Z_1}{Z_1 + Z_2} \tag{2}$$

where $Z = \rho c$, ρ is the density of the medium, and c is the acoustic velocity of the wave propagating inside of the medium. In our case, Z_1 is the acoustic impedance of the liquid, and Z_2 is the acoustic impedance of the (100) silicon substrate. An online assessment of the evaporation kinetics of the droplet is feasible because of the measurement of this reflection coefficient.

The width of the acoustical pulse is 5 ns. It corresponds to 5 times the period of the working frequency of 1 GHz. Because the wavelength λ_l in water is about 1.5 μm, one can consider that the wave propagates over a distance of 5 times the wavelength λ_l in the liquid, namely 7.5 μm. Beyond this thickness, the acoustic wave undergoes a strong attenuation. Because we process droplets of 1 μL, the corresponding diameter and height are about 1.5 mm each. The information gathered is then limited to a few micrometers inside of the drop at the bottom.

EXPERIMENTAL RESULTS

Calibration of the Acoustic Measurement Method: Water as a Reference Liquid. To calibrate our acoustic device, water is used as a reference liquid. The acoustic reflection coefficient is calculated from the density and the acoustic velocity of both silicon and water, as found in the literature. Several precautions are taken to improve the accuracy of the measurements. Temporal drifts are minimized by the use of two identical transducers, one as reference to air and the other for measurement at the silicon−liquid interface. The reference to air is first measured in each case. The adjustment factor $|R|_c$ is equal to the ratio of the peak amplitudes A_{22} and A_{11}, which are the reflection coefficients measured with each probe on each transducer.

$$|R|_c = \left(\frac{A_{22}}{A_{11}}\right)_{air} \tag{3}$$

The standardized reflection coefficient, R_{norm} at the solution (sol)−silicon interface is then deduced as

$$|R|_{norm} = \frac{(A_{22}/A_{11})_{sol}}{(A_{22}/A_{11})_{air}} \tag{4}$$

A drop of water of approximately 1 μL is deposited on the surface of the planar (100) silicon substrate. According to eq 2, the reflection coefficient at the silicon−water interface is deduced to be 0.8595. Reliability can be assessed according to the stability and the accuracy of the measurement when compared with the theoretical value; it is determined to be 0.02%.

The physical properties of the pure liquids and their studied mixtures as well as the (100) silicon substrate at a temperature of 22 °C are reported in Table 1. ρ is the density, γ is the surface tension, P_{sat} is the saturation vapor pressure, and c is the acoustic velocity. The volatility is measured through the saturation vapor pressure P_{sat}. The higher the value of P_{sat}, the more volatile the liquid is. Note that P_{sat} is given for large volumes of liquid.

Table 1. Physical Properties of Fluids and (100) Silicon at 22 °C and 1 atm

	ρ (kg·m^{-3})	γ (mN·m^{-1})	P_{sat} (kPa)	c (m·s^{-1})
water	998	72.80	2.65	1488.319[29]
(100) silicon	2330			8433.8[30]
1-butanol	809	24.67	0.80	
water + 5% 1-butanol	989	33.60	2.56	
ethanol	789	22.31	5.80	
water + 5% ethanol	988	56.41	2.81	
water + 25% ethanol	946	36.09	3.44	
water + 50% ethanol	894	28.51	4.23	

Evaporation of Drops of Pure Liquids. We focused our immediate attention on pure liquids, namely pure butanol and pure ethanol. The minimum and maximum values of relative humidity that the vapor chamber can attain are 20% and 56%, respectively; moreover, 50% was chosen as the mean RH. Acoustic measurements were made in a surrounding humidity of approximately 50%.

Pure Butanol. *Optical and Infrared Investigations.* For each liquid, we measured the contact angle, diameter, and volume of the droplets versus time and deduced $V^{2/3}$. All experiments were repeated five times to guarantee a good repeatability. The plots of contact angle and $V^{2/3}$ versus time are presented in Figure 2. The evaporation of pure 1-butanol drops can be divided into two stages: initially the contact angle decreased slightly, followed by the stage of constant contact angle during most of the evaporation time. The different values of RH used had no obvious effect on the evaporation of pure 1-butanol drops.

For a spherical cap drop, the evaporation rate[31] can be given by eq 5

$$-\left(\frac{dV}{dt}\right) = \frac{4\pi D}{\rho_L}\left(\frac{3V}{\pi\beta}\right)^{1/3}(C_s - C_\infty)f(\theta) = KV^{1/3}f(\theta) \tag{5}$$

where

$$K = \frac{4\pi^{2/3}3^{1/3}D(C_s - C_\infty)}{\rho_L\beta^{1/3}}$$

$$\beta = 2 - 3\cos\theta + \cos^3\theta$$

and V is the volume of the spherical cap drop, D is the diffusion coefficient of vapor in air, ρ_L is the liquid density of the drop, C_s and C_∞ are the vapor concentrations close to and far from the drop surface, respectively, θ is the contact angle, $f(\theta)$ is a function of the contact angle of the spherical cap given by the model of Picknett and Bexon[8]

$$f(\theta)_{\text{Picknett\&Bexon}} = \frac{1}{2}\left(\frac{C}{R_s}\right) \tag{6}$$

For $10° \le \theta < 180°$,

$$\frac{C}{R_s} = 0.00008957 + 0.6333\theta + 0.116\theta^2 - 0.08878\theta^3 + 0.01033\theta^4 \tag{7}$$

Assuming that the diffusion of vapor molecules in air is steady and that the contact angle remains constant during evaporation, eq 5 can be integrated between the initial volume V_0 $(t \to 0)$ and V_t $(t \to t)$

$$V_t^{2/3} = V_0^{2/3} - \frac{2}{3}Kf(\theta)t \tag{8}$$

The plots of $V^{2/3}$ versus time, as shown in Figure 2, are linear regardless of the conditions of RH. In the case of 56% RH, according to the slopes of our plots, $Kf(\theta)$ varies in the range of 1.42×10^{-5} to 1.69×10^{-5} cm^2/s. These values are comparable to the theoretical ones calculated from eqs 5−7, which fall in the range of 1.22×10^{-5} to 1.33×10^{-5} cm^2/s.

Figure 3 shows the evaporation process of pure 1-butanol droplets at 56% RH under the infrared camera (see Supporting Information[32] for visualization). According to the Stefan−Boltzmann law, the radiant existence of a gray body j is determined as

$$j = \varepsilon\sigma T^4 \tag{9}$$

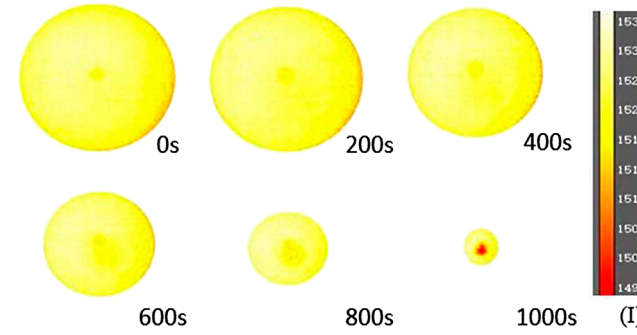

Figure 3. Snapshots from an infrared video camera of the evaporation process of a pure 1-butanol droplet at 56% RH (the corresponding video is provided in the Supporting Information[32]).

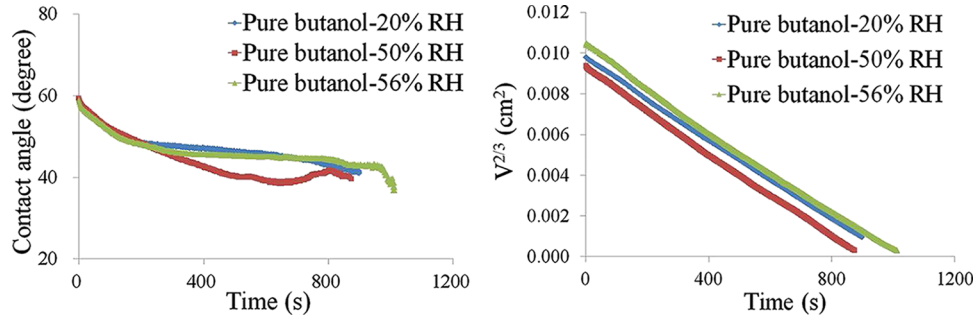

Figure 2. Evolutions of the contact angle and $V^{2/3}$ for pure 1-butanol droplets under different RH conditions versus time.

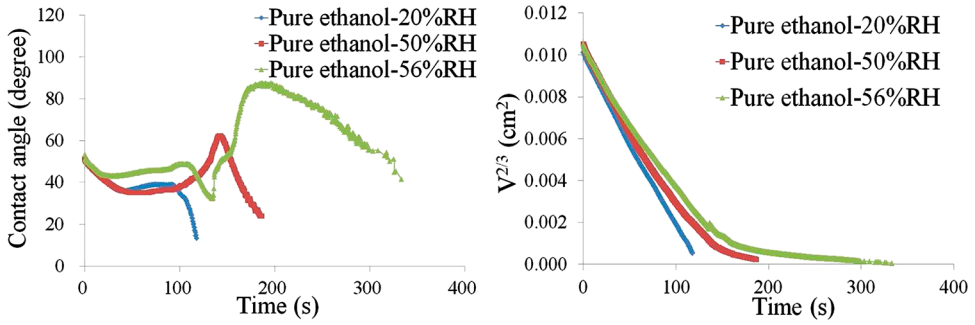

Figure 4. Evolutions of the contact angle and $V^{2/3}$ for pure ethanol droplets under different RH conditions versus time.

where σ is the Stefan−Boltzmann constant and ε and T are the emissivity and temperature of the substance, respectively. The scale in infrared thermal mapping represents the level of thermal radiation "I" received by the infrared camera. The "I" level is proportional to the radiant "j". The different colors denote different temperatures or different emissivities related to different substances. Water and alcohol in the mixture droplet have the same temperature, but the emissivity of water is higher than that of alcohol. Consequently, there is a color contrast between water and alcohol, which is visualized under the infrared camera. The normal temperature profile of a single-substance droplet is that it is coolest at the apex of droplet and warmest at the contact line, and the temperature varies from the apex to the contact line gradually. According to these infrared images in Figure 3, the color consistency at the surface until the end of evaporation indicates that the temperature of the droplet surface is almost homogeneous and there is no second liquid present in the droplet. Moreover, the phenomenon was similar under different RH conditions.

Acoustic Investigations. The reflection coefficient of the pure 1-butanol drop remained constant during the evaporation process. This acoustic measurement supports the observation made using optical and infrared techniques showing no influence of ambient humidity during evaporation. These results confirm the investigation of Seaver et al., who showed a very low hygroscopic power of a 1-butanol drop during evaporation.[33]

Pure Ethanol. *Optical and Infrared Investigations.* Figure 4 represents the evolutions of contact angle and $V^{2/3}$ of pure ethanol droplets versus time. For these three RH situations, contact angle of the pure ethanol droplet went through a quick decrease and then a constant regime at the beginning, which is similar to the evaporation of a pure butanol droplet. In the case of 20% RH, the contact angle increased slightly and then decreased until the end of evaporation after the first two stages. However, in the cases of higher RH, the contact angle rose rapidly to a maximal value. In particular, the case of 56% RH had a transition stage before the rapid rise when the contact angle decreased, and the maximal value (88°) was close to the contact angle of a pure water droplet (107°). According to Young's equation

$$\cos\theta = \frac{\gamma_{SG} - \gamma_{SL}}{\gamma_{LG}} \tag{10}$$

where γ_{SG}, γ_{SL}, and γ_{LG} are solid−vapor, solid−liquid, and liquid−vapor interfacial tensions, respectively. Owing to the high hygroscopic nature of pure ethanol, water vapor condenses on the surface of the pure ethanol droplet during evaporation. The liquid−vapor interfacial tension increases with the increase in the water−ethanol ratio of the droplet at the contact line, which leads to the rise in contact angle (eq 10). The condensation rate of water depends on the water vapor pressure of the surrounding environment. Thus, the RH can notably change the behavior of the evaporation of pure ethanol droplets. The evaporation time of a drop at 56% RH is nearly thrice that of a drop at 20% RH because the drop absorbed more water, the diffusion coefficient of which in the air is much less than that of ethanol. In addition, the plot of $V^{2/3}$ can be obviously divided into two stages with different slopes for higher relative humidity: the initial steep stage when only ethanol evaporated and then the gentle stage when the contact angle reached the maximum until the end and during which water mainly evaporated. We can conclude that the pure ethanol droplet absorbs a non-negligible quantity of water during evaporation at 50% and 56% RH, which has a significant effect on the evaporation of the pure ethanol droplet.

Contrary to the case of pure 1-butanol, the infrared thermal mapping using the infrared camera reveals heterogeneous zones during the evaporation process of a drop of pure ethanol. Figure 5 represents the infrared images in the case of 56% RH

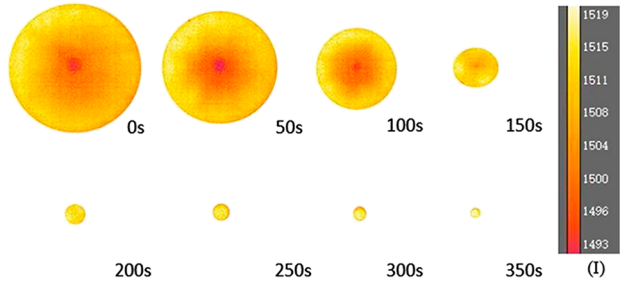

Figure 5. Snapshots from an infrared video of the evaporation process of a pure ethanol droplet at 56% RH (the corresponding video is provided in the Supporting Information[32]).

at different times (the corresponding video is provided in the Supporting Information[32]). These snapshots show that some convection cells appeared from the beginning, demonstrating the presence of liquids of different densities (ethanol and water). After 200 s, the drop became too small to allow for the distinction of convection cells; however, according to the analysis mentioned above, no ethanol was present at the drop surface and no convection cells were found. By reducing the RH to 50% and 20%, the phenomena observed were similar, the only difference being that the convection cells were weakened and less visible. Thus, the environmental RH can significantly affect the evaporation of a pure ethanol droplet, which absorbs water as soon as it is exposed in the air.

Acoustic Investigations. In the case of pure 1-butanol, we followed the evaporation kinetics of a drop of pure ethanol under the same conditions of temperature and humidity. One can see clearly that the ethanol drop undergoes progressive water loading until no more alcohol remains at the bottom of the drop, when the reflection coefficient tends toward that of water and then maintains the value (Figure 6). Notably, the high hygroscopic power of ethanol has been reported by Liu et al., who demonstrated the influence of water condensation in the evaporation of water−ethanol mixture drops.[24]

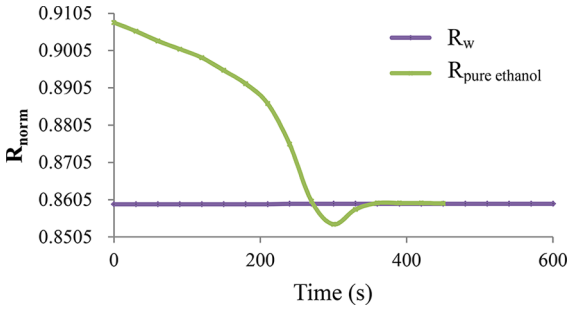

Figure 6. Kinetics of the acoustic reflection coefficient for a drop of pure ethanol.

To the best of our knowledge, there is no reference in the literature regarding the evaporation of a sessile droplet of pure ethanol. The findings presented here constitute an original result, showing that the water vapor from the ambient humidity condenses onto the droplets of pure ethanol during evaporation, and then the solution becomes a mixture of water and ethanol.

Evaporation of Drops of Binary Solutions. In the following experiments, the droplets of pure water and binary solutions were tested at a temperature of 22 °C and a hygrometry of approximately 50% with the volume of 1 μL.

Water−Butanol Mixture. *Optical and Infrared Investigations.* For the water−1-butanol mixture, the result was compared with that of pure water on the kinetics of contact angle and the plot of $V^{2/3}$. Figure 7 represents the evolutions of contact angle and $V^{2/3}$ for the pure water droplets and 5% mass concentration water−1-butanol mixture. In spite of the slight decrease at the beginning, which was due to evaporation, the contact angle of the pure water drop remained constant during most of the evaporation process and decreased abruptly at the end. Different from that of pure water, the contact angle of the water−1-butanol mixture initially decreased and then increased until the maximal value before decreasing abruptly at the end of drop life. The plot of $V^{2/3}$ of a water droplet is linear whereas that of the water−1-butanol mixture has a slight deviation at the beginning due to the evaporation of 1-butanol.

Even though the diffusion coefficient of water vapor in air (0.282 cm^2/s) is much higher than that of 1-butanol vapor (0.08 cm^2/s), the ratio of evaporation rate is still lower than the water−1-butanol component ratio. Therefore, the concentration of 1-butanol near the air−liquid interface decreased, which created a concentration gradient between the surface and bulk. To replenish the part evaporated on the surface, the 1-butanol inside of the drop flowed outward to generate convection cells. Figure 8 shows the evaporation process of water−1-butanol mixture droplets with 5% butanol mass concentration under the infrared camera (the corresponding video is provided in the Supporting Information[32]). At the beginning, the motion of convection cells is fierce and random without any thermal pattern. Because the drop evaporated at the ambient temperature, there is no large temperature gradient in the droplet. Therefore, the color difference of convection cells is due to emissivity difference, which indicates different substances, instead of temperature difference. As evaporation progressed, the convection cells became smaller and slowed down toward the contact line until they disappeared. With

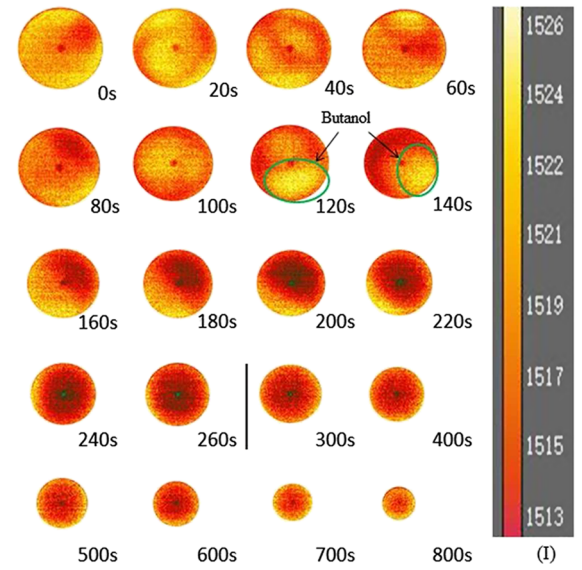

Figure 8. Snapshots from an infrared video of the evaporation process of a water−1-butanol mixture droplet containing 5 wt % 1-butanol at ambient temperature (the corresponding video is provided in the Supporting Information[32]).

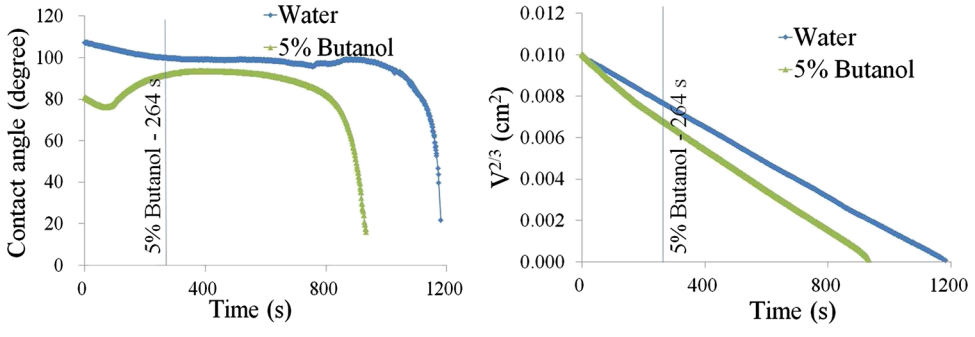

Figure 7. Evolutions of contact angle and $V^{2/3}$ for droplets of pure water and 5% mass concentrations water−1-butanol mixtures versus time.

these infrared videos, we can visually identify the time when the thermal instabilities disappeared and the color distribution on the droplet surface became stable as the moment when the 1-butanol in the droplet exhausted. The duration of 1-butanol is marked in Figure 7, where the 1-butanol disappeared at 264 s. The finish point determined by the infrared video is also the moment when the contact angle reached a maximal value close to that of water and the constant contact angle stage began.

Acoustic Investigations. From the acoustic reflection coefficient measured during the evaporation of a 5% mass concentration water−1-butanol mixture drop, one can follow the decrease in the concentration of 1-butanol inside of the drop at the liquid−substrate interface. Beforehand, the calibration curve giving the acoustic reflection coefficient as a function of mass concentration is established.

Because the limit of solubility of 1-butanol is reached for a mass concentration of approximately 7.3%, the upper limit is fixed here at C_m = 7%. Figure 9 is the result of the average of a series of three measurements performed under the same conditions. The dispersion is in the range of 0.03%.

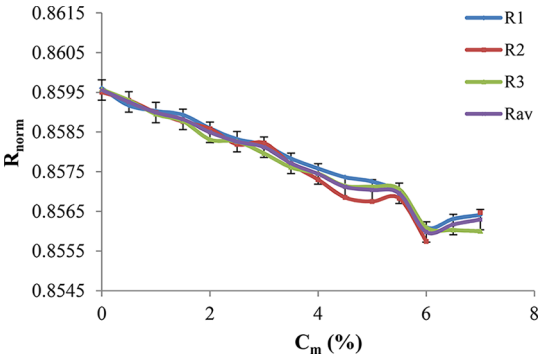

Figure 9. Calibration curve for 1-butanol at a temperature of 22 °C and a hygrometry of 50%.

Starting with a mass concentration of 5%, the alcohol concentration at the bottom of the drop during evaporation is represented in Figure 10. The curve is the average of a series of

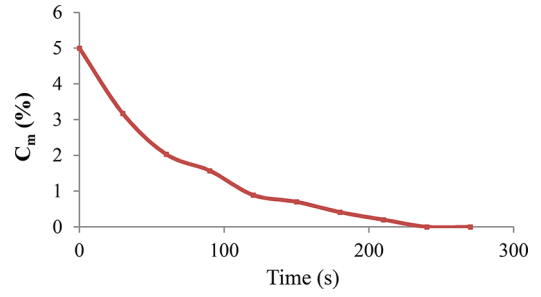

Figure 10. Mass concentration kinetics during evaporation of a droplet of 5 wt % of 1-butanol deduced from the measurement of the acoustic reflection coefficient.

five measurements from which the necessary time $t_{C=0}$ for 1-butanol concentration to decrease to zero can be determined. This time is estimated to be t_{C0} = 220 ± 15 s.

Evaporation of Water−Ethanol Mixtures. *Optical and Infrared Investigations.* Equally, Figure 11 displays the evolutions of contact angle and $V^{2/3}$ for droplets of pure water and 5%, 25%, and 50% ethanol mass concentrations of water−ethanol mixtures. Because of the tiny mass concentration of ethanol, the contact angle of a droplet containing 5 wt % of ethanol developed versus time varied analogously as that of pure water. With the increase in mass concentration, the behavior of the droplets with 25 and 50 wt % of ethanol appears similar to that of water−1-butanol mixture, and the evolutions of contact angle can be divided into the same four stages: decline, increase, smooth, and decrease at the end. From the online[32] infrared videos (Figures 12 and 13), we can notice the appearance of the same thermal instabilities as in the case of water−1-butanol mixture and also identify the time when convection cells disappear while color distribution on the droplet surface becomes stable as shown in Figure 11. On account of the very short life time of convection cells, the infrared video for a droplet of 5 wt % water−ethanol mixture is not shown here. The estimated life time of ethanol are 5, 55, and 100 s for 5, 25, and 50 wt % water−ethanol mixtures, respectively. Along with the contact angle evolutions, similar to the water−1-butanol mixtures, the finish points are situated at the maximal value of the contact angle and at the end of the increase stage for 25 and 50 wt % concentrations. The droplets of the water−ethanol mixture with high ethanol mass concentration behaved the same as those of water−1-butanol mixture, whereas the behavior of the droplets with low ethanol mass concentration appeared similar to that of pure water. For the plot of $V^{2/3}$, 5 wt % water−ethanol had the same linearity as pure water because of the very low ethanol concentration. For both 25% and 50% concentrations, the plot of $V^{2/3}$ has two different slopes: the first steep stage related to the quick evaporation of ethanol and the second more gentle stage. The steep stage extends with higher ethanol concentration. During the second stage, the plots of $V^{2/3}$ of all the water−ethanol mixtures have a similar regression coefficient and the contact angles stay nearly constant. According to eqs 5 and 8, $(2/3)Kf(\theta)$ represents the regression coefficient of plot of $V^{2/3}$ and the same value indicates no change in density as well as the component. Hence, water mainly evaporates in the second stage.

Acoustic Investigations. The ethanol concentration is monitored during the evaporation of a drop for each of the mass concentrations of ethanol of 5%, 25%, 50%, and 100%. In the same manner as 1-butanol, the reflection coefficient is first measured during the evaporation kinetics. From the calibration curve giving the reflection coefficient as a function of the mass concentration of ethanol, shown in Figure 14, the concentration evolution of alcohol is then transcribed as shown in Figure 15. The results are the average of a series of three measurements.

Also reported in Figure 14 is the analytical evolution as a function of the mass concentration of ethanol obtained from Vatandas et al.[34] There is a good agreement between the theoretical values and the measured ones within a confidence range of about 0.75%.

From Figure 15, one can extract relevant parameters such as the time t_{C0} necessary for the concentration to decrease to zero. The precision on t_{C0} is approximately 15 s. Table 2 summarizes the t_{C0} times for the different concentrations of ethanol and 1-butanol.

Comparison between the Acoustics and Infrared Observations. Acoustics provides information on the manner by which alcohol is exhausted from the bottom of the drop, whereas infrared observation is related to the disappearance of alcohol from the surface of the drop. The necessary time for

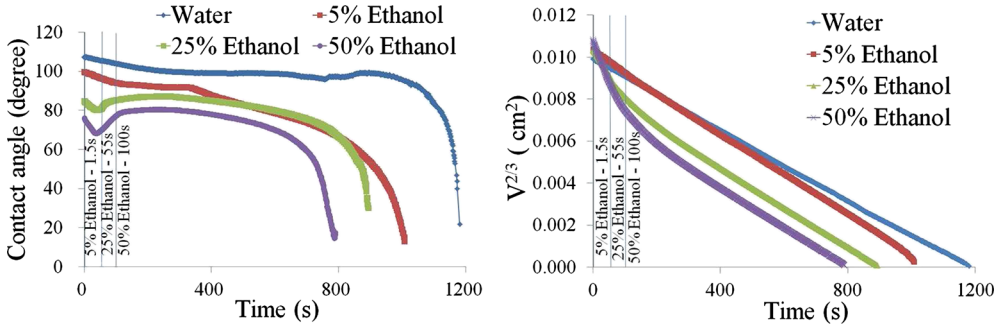

Figure 11. Evolution of contact angle and $V^{2/3}$ for droplets of pure water and droplets of 5%, 25%, and 50% mass concentrations of water−ethanol mixtures versus time.

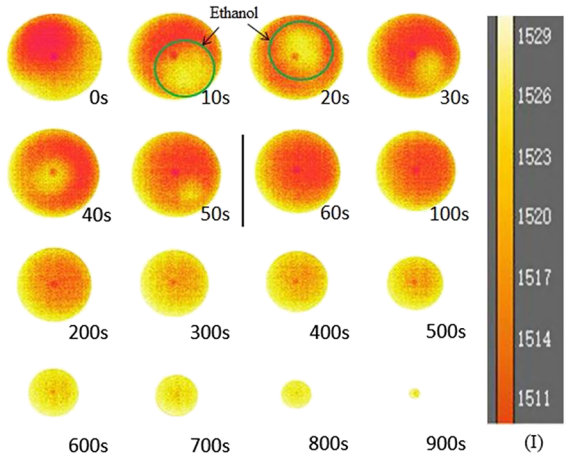

Figure 12. Snapshots from an infrared video of the evaporation process of a water−ethanol mixture droplet containing 25 wt % ethanol at ambient temperature (the corresponding video is provided in the Supporting Information[32]).

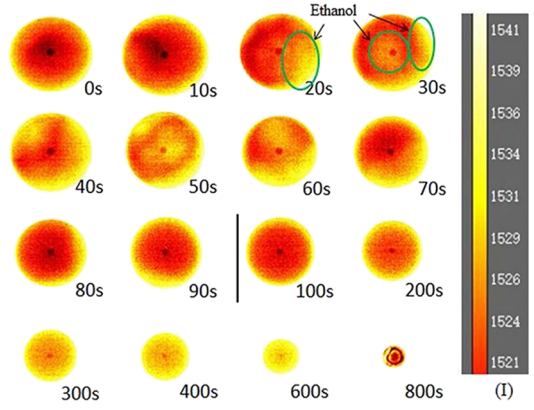

Figure 13. Snapshots from an infrared video of the evaporation process of a water−ethanol mixture droplet containing 50 wt % ethanol at ambient temperature (the corresponding video is provided in the Supporting Information[32]).

alcohol to exhaust from the bottom and from the surface of the drop is reported in Table 3.

The times estimated by these two methods are comparable in the case of 1-butanol with a mass concentration of 5%. However, this is not the same for any ethanol concentration. The possible reasons are the difference in volatility between ethanol and 1-butanol. At the beginning, the contact angle of the water−ethanol mixture droplet decreased because of

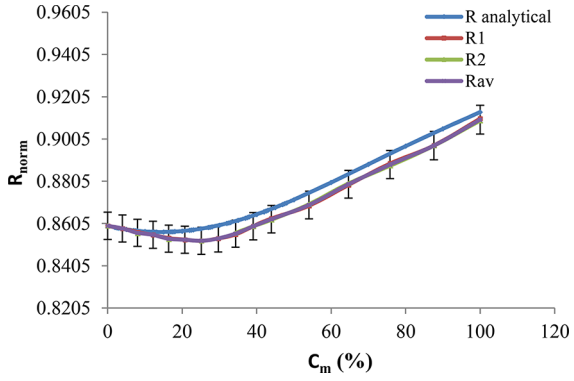

Figure 14. Calibration curve for ethanol at a temperature of 22 °C and a hygrometry of 50%.

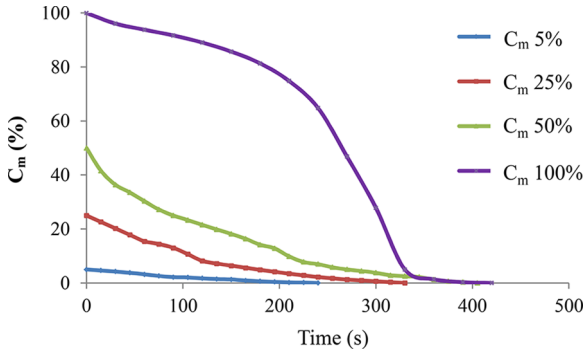

Figure 15. Mass concentration kinetics during the evaporation of droplets of 5%, 25%, 50%, and 100% of ethanol deduced from the measurement of the acoustic reflection coefficient at 22 °C.

Table 2. t_{C0} for the Different Concentrations of Ethanol and 1-Butanol

	t_{C0} (s)	
C_m (%)	ethanol	1-butanol
5	230 ± 15	220 ± 15
25	330 ± 15	
50	405 ± 15	
100	420 ± 15	

evaporation until the contact angle reached the receding angle of the mixture solution. Then, the contact line began to retract, and the thermodynamic equilibrium of the three interfaces was broken. Because of high volatility, ethanol evaporates faster than water, which leads to a decrease in ethanol concentration at the air−liquid interface and an

Table 3. Comparison between the Visual and Acoustic Methods

	5 wt % ethanol	25 wt % ethanol	50 wt % ethanol	5 wt % 1-butanol
visual method	1.5 s	55 s	100 s	264 s
acoustic method	230 ± 15 s	330 ± 15 s	405 ± 15 s	220 ± 15 s

increase in the surface tension of the droplet from the beginning. Hence, the contact angle increased since the disequilibrium of the three interfaces. The ethanol concentration gradient was created between the surface and the interior of the droplet, which is the origin of convective flow. Therefore, the ethanol evaporated on the surface was replenished by convective flow, which generated the convection cells observed under the infrared camera and diffusion of ethanol molecules. When the total ethanol concentration and the concentration gradient became so weak that the convective flow could not be engendered, the evaporation of ethanol on the droplet surface was controlled by its diffusion in the droplet. It is because the ethanol molecules need time to diffuse from the bottom to the surface of the droplet and the diffusion coefficient of ethanol molecules in water (1.22×10^{-9} m^2/s) is much lower than that in air (1.15×10^{-5} m^2/s). Thus, the ethanol−water ratio stayed at a very low value on the surface of the droplet, which could not be distinguished by the infrared camera, and the contact angle stayed constant. The evaporation process is similar for the cases of 25 and 50 wt % ethanol concentrations, except for the case of 5 wt % whose ethanol concentration on the droplet surface is so low that it decreased quickly and the evaporation of ethanol was mostly controlled by diffusion in the droplet. However, during the evaporation controlled by diffusion in the droplet, there was still a certain quantity of ethanol in the droplet which could be detected by the acoustic method. That is the reason for the large difference of exhaustion time of ethanol in the droplet estimated between the visual and acoustic methods. In the case of 5 wt % water−1-butanol mixture, even the same concentration as 5 wt % water−ethanol mixture, the droplet had the same evaporation process as that of 25 and 50 wt % water−ethanol mixture. Owing to the low evaporation rate of butanol, the decrease in 1-butanol−water ratio on the droplet surface was much slower than that of the water−ethanol mixture, which can be demonstrated by the smooth increasing curvature of contact angle during the second stage. Thence, the concentration gradient remained the same much longer, and the convective flows were generated continuously, which was distinct under the infrared camera. Even though the convective flows became weak, the supply of diffusion (0.93×10^{-9} m^2/s) in the droplet maintained the 1-butanol−water ratio on the surface at a certain value, which could be detected by the infrared camera, due to the low evaporation rate of 1-butanol. Consequently, the exhaustion times of 1-butanol in the droplet estimated by the two methods are close. Because the exhaustion of 1-butanol begins from the bottom of the droplet on account of diffusion, the exhaustion time estimated by the acoustic method is shorter than the visual method. However, at the same concentration, the exhaustion times of alcohol estimated by the acoustic method for water−ethanol and water−1-butanol mixture are very close, which implies that the diffusion of alcohol molecules is dominant during evaporation, and with or without convection, there is no effect on the evaporation of alcohol in a mixture droplet.

CONCLUSIONS

For the first time, the acoustic method was applied to track the alcohol concentration at the bottom of a droplet of binary solution during evaporation. Using the pre-established acoustic reflection coefficient as a function of mass concentration, the alcohol concentration kinetics can be monitored versus time. From the infrared images, the color distribution resulting from the temperature and emissivity gradients is correlated with the existence of alcohol on the drop surface.

No ambient humidity influence is observed in the behavior of the contact angle and $V^{2/3}$ of a drop of pure 1-butanol during evaporation. In addition, the temperature at the surface remains constant and the acoustic reflection coefficient also remained constant during the process, that is, no change in 1-butanol concentration occurred. These results confirm the very low hygroscopic power of a drop of 1-butanol during evaporation.

Because of the high hygroscopic nature of ethanol, evaporation of a drop of pure ethanol is largely impacted by the RH. Because of the absorption of water, the ethanol droplet becomes a water−ethanol mixture and the convection cells appear from the beginning. The kinetics of the acoustic reflection coefficient results in a decreasing trend of the ethanol concentration until reaching the acoustic reflection coefficient of water. These results showed that water vapor coming from ambient humidity condenses onto the droplets of pure ethanol during evaporation and the solution becomes a mixture of water and ethanol. As a consequence of high volatility, firstly the ethanol evaporated and exhausted, and then the absorbed water continued to evaporate through the end.

The exhaustion time of ethanol in a drop estimated by the acoustic method is always much shorter than that estimated by the visual method at three different ethanol concentrations. However, in the case of water−butanol mixture, both methods bear the same result. This can be probably explained by the difference in the water−alcohol ratio on the drop surface because of difference in volatility between ethanol and butanol.

AUTHOR INFORMATION

Corresponding Author

*E-mail: souad.harmand@univ-valenciennes.fr.

Notes

The authors declare no competing financial interest.

ACKNOWLEDGMENTS

The authors would like to acknowledge the support of the CE2I-CPER, the FEDER and “Hauts de France” Institutes for this work.

REFERENCES

(1) Deegan, R. D.; Bakajin, O.; Dupont, T. F.; Huber, G.; Nagel, S. R; Witten, T. A. Contact line deposits in an evaporating drop. *Phys. Rev. E: Stat. Phys., Plasmas, Fluids, Relat. Interdiscip. Top.* **2000**, *62*, 756.

(2) Hu, H.; Larson, R. G. Marangoni effect reverses coffee-ring depositions. *J. Phys. Chem. B* **2006**, *110*, 7090−7094.

(3) Ristenpart, W. D.; Kim, P. G.; Domingues, C.; Wan, J.; Stone, H. A. Influence of substrate conductivity on circulation reversal in evaporating drops. *Phys. Rev. Lett.* **2007**, *99*, 234502.
(4) Kelly-Zion, P. L.; Pursell, C. J.; Vaidya, S.; Batra, J. Evaporation of sessile drops under combined diffusion and natural convection. *Colloids Surf., A* **2011**, *381*, 31−36.
(5) Nguyen, T. A. H.; Nguyen, A. V.; Hampton, M. A.; Xu, Z. P.; Huang, L.; Rudolph, V. Theoretical and experimental analysis of droplet evaporation on solid surfaces. *Chem. Eng. Sci.* **2012**, *69*, 522−529.
(6) Carle, F.; Sobac, B.; Brutin, D. Experimental evidence of the atmospheric convective transport contribution to sessile droplet evaporation. *Appl. Phys. Lett.* **2013**, *102*, 061603.
(7) Gatapova, E. Y.; Semenov, A. A.; Zaitsev, D. V.; Kabov, O. A. Evaporation of a sessile water drop on a heated surface with controlled wettability. *Colloids Surf., A* **2014**, *441*, 776−785.
(8) Picknett, R. G.; Bexon, R. The evaporation of sessile or pendant drops in still air. *J. Colloid Interface Sci.* **1977**, *61*, 336−350.
(9) Kneer, R.; Schneider, M.; Noll, B.; Wittig, S. Diffusion controlled evaporation of a multicomponent droplet: Theoretical studies on the importance of variable liquid properties. *Int. J. Heat Mass Transfer* **1993**, *36*, 2403−2415.
(10) Erbil, H. Y.; Meric, R. A. Evaporation of sessile drops on polymer surfaces: Ellipsoidal cap geometry. *J. Phys. Chem. B* **1997**, *101*, 6867−6873.
(11) Masoud, H.; Felske, J. D. Analytical solution for inviscid flow inside an evaporating sessile drop. *Phys. Rev. E: Stat., Nonlinear, Soft Matter Phys.* **2009**, *79*, 016301.
(12) Sefiane, K.; Bennacer, R. An expression for droplet evaporation incorporating thermal effects. *J. Fluid Mech.* **2011**, *667*, 260−271.
(13) Kawase, T.; Sirringhaus, H.; Friend, R. H.; Shimoda, T. Inkjet printed via-hole interconnections and resistors for all-polymer transistor circuits. *Adv. Mater.* **2001**, *13*, 1601−1605.
(14) de Gans, B.-J.; Duineveld, P. C.; Schubert, U. S. Inkjet printing of polymers: State of the art and future developments. *Adv. Mater.* **2004**, *16*, 203−213.
(15) Wang, W.; Lin, J.; Schwartz, D. C. Scanning force microscopy of DNA molecules elongated by convective fluid flow in an evaporating droplet. *Biophys. J.* **1998**, *75*, 513−520.
(16) Chopra, M.; Li, L.; Hu, H.; Burns, M. A.; Larson, R. G. DNA molecular configurations in an evaporating droplet near a glass surface. *J. Rheol.* **2003**, *47*, 1111.
(17) Saito, M.; Sato, M.; Suzuki, I. Evaporation and combustion of a single fuel droplet in acoustic fields. *Fuel* **1994**, *73*, 349−353.
(18) Park, C.-W.; Kaviany, M. Evaporation-combustion affected by in-cylinder, reciprocating porous regenerator. *J. Heat Transfer* **2002**, *124*, 184−194.
(19) Wu, S.-C. Study of self-rewetting fluid applied to loop heat pipe. *Int. J. Therm. Sci.* **2015**, *98*, 374−380.
(20) Su, X.; Zhang, M.; Han, W.; Guo, X. Enhancement of heat transport in oscillating heat pipe with ternary fluid. *Int. J. Heat Mass Transfer* **2015**, *87*, 258−264.
(21) Sefiane, K.; Tadrist, L.; Douglas, M. Experimental study of evaporating water−ethanol mixture sessile drop: Influence of concentration. *Int. J. Heat Mass Transfer* **2003**, *46*, 4527−4534.
(22) Christy, J. R. E.; Hamamoto, Y.; Sefiane, K. Flow transition within an evaporating binary mixture sessile drop. *Phys. Rev. Lett.* **2011**, *106*, 205701.
(23) O'Hare, K. D.; Spedding, P. L. Evaporation of a binary liquid mixture. *Chem. Eng. J.* **1992**, *48*, 1−9.
(24) Liu, C.; Bonaccurso, E.; Butt, H.-J. Evaporation of sessile water/ethanol drops in a controlled environment. *Phys. Chem. Chem. Phys.* **2008**, *10*, 7150−7157.
(25) Saad, N.; Dufour, R.; Campistron, P.; Nassar, G.; Carlier, J.; Harnois, M.; Merheb, B.; Boukherroub, R.; Senez, V.; Gao, J.; Thomy, V.; Ajaka, M.; Nongaillard, B. Characterization of the state of a droplet on a micro-textured silicon wafer using ultrasound. *J. Appl. Phys.* **2012**, *112*, 104908.
(26) Dufour, R.; Saad, N.; Carlier, J.; Campistron, P.; Nassar, G.; Toubal, M.; Boukherroub, R.; Senez, V.; Nongaillard, B.; Thomy, V. Acoustic Tracking of Cassie to Wenzel Wetting Transitions. *Langmuir* **2013**, *29*, 13129−13134.
(27) Carlier, J.; Toubal, M.; Li, S.; Campistron, P.; Callens, D.; Thomy, V.; Senez, V.; Nongaillard, B. High frequency acoustic reflectometry for solid/liquid interface characterization: Application to droplet evaporation. *Phys. Procedia* **2015**, *70*, 459−462.
(28) Li, S.; Lamant, S.; Carlier, J.; Toubal, M.; Campistron, P.; Xu, X.; Vereecke, G.; Senez, V.; Thomy, V.; Nongaillard, B. High frequency acoustic for nanostructures wetting characterization. *Langmuir* **2014**, *30*, 7601−7608.
(29) Bilaniuk, N.; Wong, G. S. K. Speed of sound in pure water as a function of temperature. *J. Acoust. Soc. Am.* **1993**, *93*, 1609.
(30) Nikanorov, S. P.; Burenkov, Y. A.; Stepanov, A. V. Elastic properties of Si. *Sov. Phys. Solid State* **1972**, *13*, 2516.
(31) Erbil, H. Y.; McHale, G.; Newton, M. I. Drop evaporation on solid surfaces: Constant contact angle mode. *Langmuir* **2002**, *18*, 2636−2641.
(32) Movies of the process are available online at https://www.youtube.com/channel/UCAEkDNQpD5psOHkLOGwuVRw.
(33) Seaver, M.; Galloway, A.; Manuccia, T. J. Water Condensation onto Evaporating Drop of 1-Butanol. *Aerosol Sci. Technol.* **1990**, *12*, 741−744.
(34) Vatandas, M.; Koc, A. B.; Koc, C. Ultrasonic velocity measurements in ethanol−water and methanol−water mixtures. *Eur. Food Res. Technol.* **2007**, *225*, 525−532.